THE ASTROPHYSICAL JOURNAL, 354:556–567, 1990 May 10

DETECTION OF WIDESPREAD STRONG METHANOL MASERS AT 44 GHz

AUBREY D. HASCHICK
Haystack Observatory[1]
KARL M. MENTEN
Harvard-Smithsonian Center for Astrophysics
AND
WILLEM A. BAAN
Arecibo Observatory[2]
Received 1989 September 1; accepted 1989 November 15

ABSTRACT

The Haystack Observatory 37 m antenna was used to search for emission from the 44 GHz $7_0 \rightarrow 6_1 A^+$ transition of interstellar methanol toward 50 galactic star-forming regions. The line was detected toward half the observed sources. Several of these regions were also observed in the 36 GHz $4_{-1} \rightarrow 3_0 E$ line. In most sources, the detected emission shows one or more narrow components indicating maser action. The spectral appearance and spatial distribution of these methanol masers closely resembles the properties of the well-studied 25 GHz methanol masers: in some cases, distances between individual methanol maser components are of order 1 pc. Unlike the now well-studied 12 GHz methanol masers, these masers appear well separated from OH/H_2O maser centers and compact H II regions.

Subject headings: interstellar: molecules — line identifications — nebulae: H II regions — radio sources: lines — stars: formation

I. INTRODUCTION

Recently, various centimeter- and millimeter-wave transitions of methanol have been found to show maser action toward a large number of interstellar sources. In particular, maser emission in the $7_0 \rightarrow 6_1 A^+$ transition near 44 GHz has been reported toward the star-forming regions Orion-KL (Ohishi 1984), Sgr B2, and W51 (Morimoto, Ohishi, and Kanzawa 1985). Due to the lack of more extensive data, the 44 GHz masers at first seem difficult to classify. They certainly show a number of characteristics of class A methanol masers (Batrla *et al.* 1987), which by definition are masing in the series of $J_{k=2} \rightarrow J_{k=1}$ E transitions near 25 GHz (Menten *et al.* 1986*a*): Like these, the 44 GHz masers only show a few spike features often superposed on broad thermal emission. In particular toward Sgr B2, extensive offset measurements have shown that individual maser spikes arise from different locations offset from the peaks of the thermal methanol emission and offset from other molecular maser centers (Morimoto, Ohishi, and Kanzawa 1985).

Despite the mentioned similarities, some facts indicate that there is not a one-to-one correspondence between 44 GHz and 25 GHz maser sources. For example, there seem to be no 25 GHz masers present in Sgr B2 (Menten *et al.* 1986*a*), and the 25 and 44 GHz spectra observed toward Orion-KL differ markedly.

Other methanol masers have also been found to show class A–like properties, including the $4_{-1} \rightarrow 3_0 E$, $5_{-1} \rightarrow 4_0 E$, and $8_0 \rightarrow 7_1 A^+$ lines at 36, 84, and 95 GHz, respectively (Morimoto, Ohishi, and Kanzawa 1985; Haschick and Baan 1989; Batrla and Menten 1988; Ohishi *et al.* 1986; Plambeck and Wright 1988). To illuminate the relationships among all these different methanol masers, we used the Haystack Observatory 37 m antenna to make a survey in the 44 GHz line.

II. OBSERVATIONS

The observations were made in 1988 January, April, September, and October using the Haystack Observatory 37 m antenna near Westford, MA. A 35.5–49 GHz tunable maser amplifier receiver was used at 44.06943 GHz, the rest frequency of the $7_0 \rightarrow 6_1 A^+$ transition, with typical system temperatures between 150 and 250 K. The spectrometer, an autocorrelator, was operated with a bandwidth of 6.67 MHz split into 1024 channels, or with 13.3 MHz bandwidth and 512 channels. This corresponds to velocity resolutions of 0.065 and 0.26 km s^{-1}, respectively. The data were corrected for atmospheric absorption and elevation dependent gain variations. At 44 GHz the beamwidth is 46″, the aperture efficiency η_A is 0.09, and the main-beam efficiency η_M is 0.11. A corrected antenna temperature T_A^* of 1 K corresponds to a flux density of 31 Jy. Toward selected sources we also measured the $4_{-1} \rightarrow 3_0 E$ transition at 36.16924 GHz. At this frequency, the beamwidth is 56″ and $\eta_A = 0.14$ and $\eta_M = 0.17$; a T_A^* of 1 K corresponds to 19 Jy. The pointing errors were estimated to be less than 15″. Antenna temperatures were determined relative to a noise tube, which is calibrated by comparison with a room temperature hot load and a cold load at liquid nitrogen temperature. We estimate that our absolute calibration is typically good to 25%. For low declination sources, most notably Sgr A, Sgr B2, and NGC 6334, the absolute calibration is more uncertain and estimated to be accurate to within only 50%.

III. RESULTS AND DISCUSSION

a) General Properties of the Observed Emission

The results of our observations are shown in Figures 1–10 and Tables 1 and 2. In Figure 1 we present spectra of sources

[1] Radio astronomy at the Haystack Observatory of the Northeast Radio Observatory Corporation (NEROC) is supported by a grant from the National Science Foundation.
[2] Arecibo Observatory is part of the National Astronomy and Ionosphere Center operated by Cornell University under contract with the National Science Foundation.

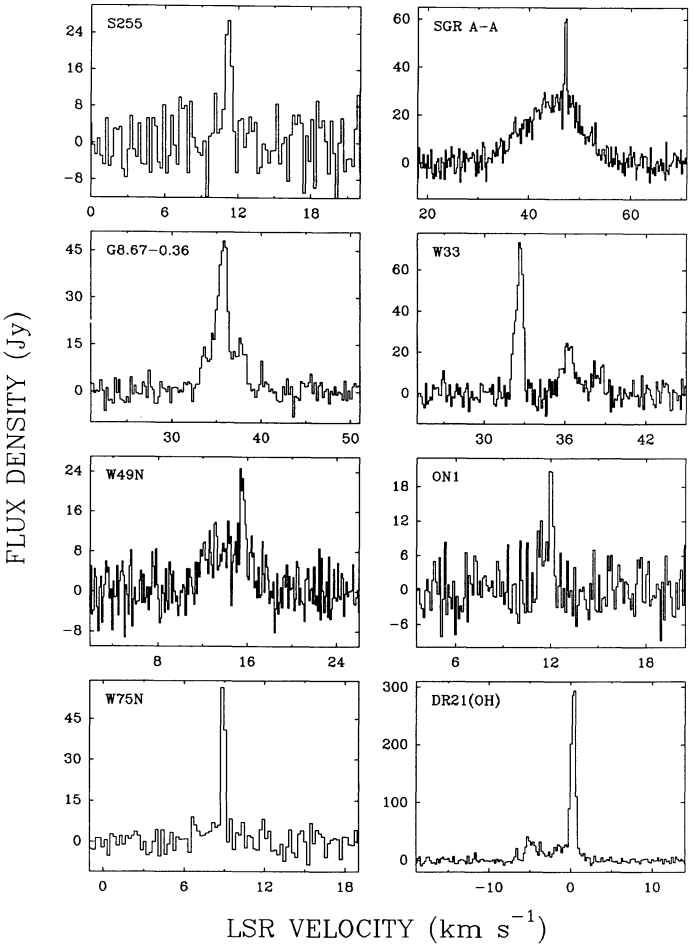

FIG. 1.—Spectra of the $7_0 \rightarrow 6_1\ A^+$ transition of CH_3OH observed toward various galactic star-forming regions. The velocity resolution is 0.11 km s^{-1} for the W33-Met, W49N, and ON1 spectra and 0.22 km s^{-1} in all other cases.

that clearly show narrow emission features indicating maser action in the $7_0 \rightarrow 6_1\ A^+$ line. Toward a number of sources also, broad, most likely thermal, emission is observed. Figures 2 and 4 show spectra of the $7_0 \rightarrow 6_1\ A^+$ and $4_{-1} \rightarrow 3_0\ E$ transitions for the sources toward which both lines were observed by us. The $7_0 \rightarrow 6_1\ A^+$ spectra displayed in Figure 3 in general have a lower signal-to-noise ratio than those shown in Figures 1 and 2, and in several cases it is difficult to decide whether narrow features are present. Around some of the positions listed in Table 1 offset measurements, typically with half-beam spacing, were performed in order to obtain information on the emission distribution and allow position determinations.

In the following we shall refer to narrow, often intense, spectral features ($\Delta v \approx 0.2$–0.7 km s^{-1}) as "maser emission." In § IIIc we shall give a number of arguments to support this classification. The terms "broad" and "thermal" emission will be used interchangeably to describe wider emission components having line widths (typically > 2 km s^{-1}) that are comparable to the Δv values observed for many other molecules toward the sources in question.

b) *Notes on Selected Sources that Show Maser Emission*

In the following we comment in some detail on a number of sources toward which clearly narrow maser features are seen. In particular, we want to compare the observed emission in the $7_0 \rightarrow 6_1\ A^+$ (and in some cases also in the $4_{-1} \rightarrow 3_0\ E$) transition with emission from previously observed maser and non-maser methanol transitions and emission from other molecules.

i) *Orion-KL*

The KL region in Orion is the first source toward which interstellar methanol masers were observed: The 25 GHz $J_{k=2} \rightarrow J_{k=1}\ E$ ($J = 4, 5, 6, 7, 8$) transitions were first detected by Barrett, Schwartz, and Waters (1971). Their maser nature was directly proven by the interferometric measurements of Matsakis *et al.* (1980), who showed that the emission arises from ≈ 10 individual spots that are scattered over a $\approx 25'' \times 40''$ area. Thermal emission from hundreds of other CH_3OH lines has in the meanwhile been observed toward Orion-KL and been shown to arise from a compact warm methanol emission core (MEC) situated near the well-studied "hot core" (Menten *et al.* 1986*b*, 1988*c*; Wilson *et al.* 1989). Interferometric observations of the 95 GHz $8_0 \rightarrow 7_1\ A^+$ transition (Plambeck and Wright 1988) show, in addition to (most

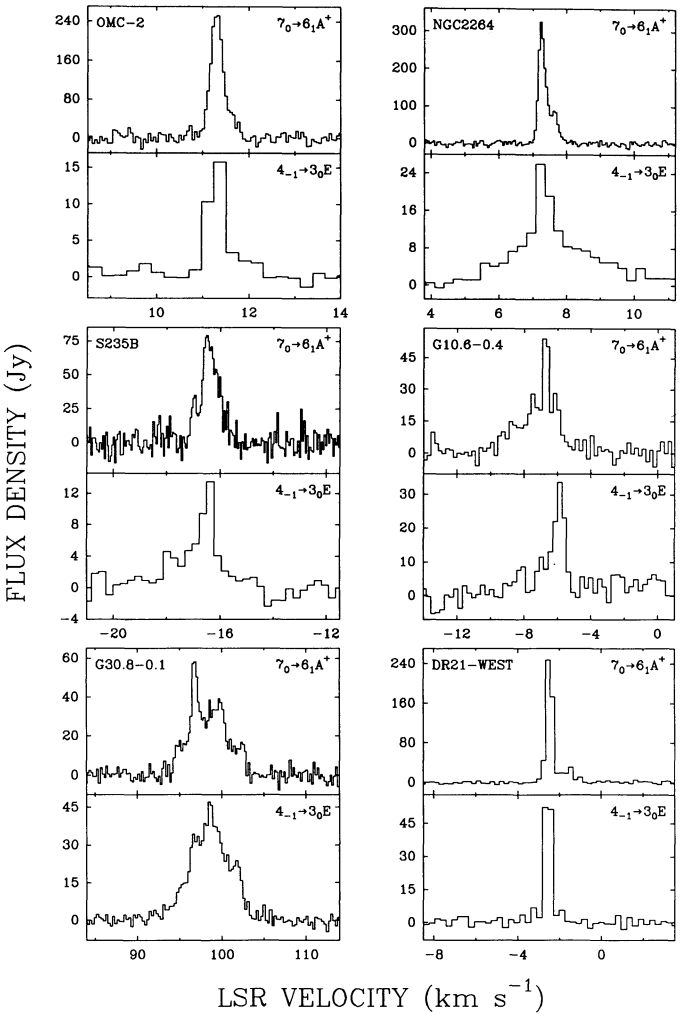

FIG. 2.—For a number of sources that show signs of maser action in both the 44 GHz $7_0 \rightarrow 6_1\ A^+$ and the 36 GHz $4_{-1} \rightarrow 3_0\ E$ transitions of CH_3OH, spectra of these transitions are shown. For each source, the *lower* panel shows the respective $4_{-1} \rightarrow 3_0\ E$ spectrum with a velocity resolution of 0.27 km s^{-1} in each case. The $7_0 \rightarrow 6_1\ A^+$ spectra, shown in the *upper* panels, have a velocity resolution of 0.055 km s^{-1} for the sources OMC–2, NGC 2264, and S235 and 0.22 km s^{-1} for the other sources.

TABLE 1

LINE PARAMETERS DETERMINED FROM $7_0 \rightarrow 6_1$ A^+ OBSERVATIONS

Source	α_{1950}	δ_{1950}	$\int S\,dv$ (Jy km s^{-1})	v_{LSR} (km s^{-1})	Δv (km s^{-1})	Notes
W3(OH)	02^{h}23^{m}17^s.3	61°38′58″	4.2(0.9)	−46.49(0.09)	0.8(0.2)	
Orion-KL	05 32 47.0	−05 24 23	19.2(0.9)	8.57(0.01)	0.22(0.08)	1
			77(3)	8.3(0.1)	3.6(0.2)	
Orion-S6	05 32 44.8	−05 26 00	23(2)	6.7(0.1)	2.6(0.3)	
OMC-2	05 32 59.8	−05 11 29	86(2)	11.30(0.01)	0.31(0.01)	2
			10(2)	11.67(0.02)	0.24(0.05)	
S235	05 37 31.8	35 40 18	57(3)	−16.38(0.02)	0.74(0.04)	2
			4.4(1.3)	−17.01(0.02)	0.17(0.04)	
S255 (0, 44″)	06 10 01.0	18 00 44	17(3)	11.18(0.05)	0.57(0.10)	
NGC 2264	06 38 24.9	09 32 28	63(3)	7.24(0.01)	0.21(0.01)	2
			44(4)	7.52(0.02)	0.46(0.03)	
NGC 6334-F	17 17 32.2	−35 44 04	150(30)	−6.1(0.5)	5.4(1.1)	
NGC 6334-I(N)	17 17 33.0	−35 42 04	...	...	...	3
Sgr A–F	17 42 27.4	−29 02 18	200(30)	21(1)	14(2)	
Sgr A–A	17 42 41.3	−28 58 18	312(10)	44.5(0.2)	12.5(0.5)	
			20(2)	47.19(0.02)	0.42(0.05)	
Sgr B2	17 44 10.6	−28 22 05	390(30)	63(1)	20(2)	
G8.67−0.36	18 03 19.0	−21 37 59	19(2)	33.92(0.12)	1.5(0.2)	4
			68(3)	35.71(0.02)	1.3(0.1)	
			21(2)	37.73(0.07)	1.2(0.2)	
G10.6−0.4	18 07 30.5	−19 56 28	≈88	...	...	5, 6
W33-Met	18 11 15.7	−17 56 53	47(2)	32.64(0.01)	0.63(0.03)	2
			29(3)	36.28(0.07)	1.3(0.2)	
G30.8−0.1	18 45 11.0	−01 57 57	24(3)	95.15(0.09)	1.4(0.2)	
			48(6)	96.81(0.02)	0.94(0.09)	
			133(9)	99.19(0.08)	3.5(0.3)	
			13(3)	102.43(0.07)	0.9(0.2)	
G34.3+0.2	18 50 46.2	01 11 12	20(3)	56.41(0.06)	1.0(0.2)	
			16(3)	58.26(0.11)	1.3(0.3)	7
W49N	19 07 49.8	09 01 17	34(4)	14.0(0.3)	4.1(0.5)	2
			9(2)	15.57(0.04)	0.48(0.09)	
W51 e_1/e_2	19 21 26.2	14 24 43	104(4)	48.88(0.02)	1.17(0.05)	
			221(9)	55.4(0.1)	7.2(0.4)	
W51-Met1	19 21 26.2	14 23 32	16(3)	56.0(0.1)	1.1(0.2)	
W51-Met2	19 21 28.8	14 23 47	6(1)	52.37(0.06)	0.60(0.13)	
			15(1)	54.04(0.03)	0.61(0.07)	
			21(1)	56.67(0.01)	0.37(0.02)	
W51-Met3	19 21 27.5	14 23 52	19(6)	53.95(0.09)	1.2(0.8)	
			10(2)	56.63(0.05)	0.46(0.09)	
W51-Met4	19 21 25.6	14 25 41	48(7)	64.4(0.2)	2.6(0.4)	
W51-Met5	19 21 20.5	14 24 12	14(2)	66.72(0.02)	0.29(0.15)	
ON1	20 08 09.9	31 22 42	4.8(1.4)	11.42(0.08)	0.49(0.17)	2
			6.9(1.2)	12.04(0.02)	0.28(0.06)	
W75N(0, 22″)	20 36 50.4	42 27 23	23.1(1.4)	8.92(0.01)	0.32(0.04)	8
DR 21–West	20 37 07.6	42 08 46	99(2)	−2.47(0.01)	0.35(0.01)	
			26(3)	−1.95(0.09)	1.6(0.2)	
			5.8(1.0)	−1.50(0.02)	0.22(0.07)	
DR 21	20 37 13.0	42 08 50	24(5)	−3.8(0.3)	2.6(0.7)	
DR 21 (OH)	20 37 13.8	42 12 13	60(5)	−4.8(0.1)	1.9(0.2)	9
			58(8)	−1.1(0.2)	2.6(0.4)	
			211(5)	0.36(0.01)	0.66(0.1)	
S140	22 17 41.2	63 03 43	12(3)	−8.22(0.07)	0.7(0.2)	
NGC 7538S	23 11 36.1	61 10 30	63(5)	−55.6(0.5)	5.2(0.5)	

NOTES.—Errors are 1 σ deviations determined by Gaussian fits. The spectra were obtained with a velocity resolution of 0.22 km s^{-1}, except where noted. Toward a number of regions, the positions of the 25 GHz $J_2 \rightarrow J_1$ E CH_3OH masers determined by Menten *et al.* 1986*a* were observed. In these cases, "-Met" has been appended to the source name.

NOTES FOR INDIVIDUAL SOURCES.—(1) Two independent Gaussians fitted. (2) Velocity resolution 0.055 km s^{-1}. (3) Complex profile: blend of several strong maser components and possible broad emission. See text for details. (4) Complex profile: additional components may be present. (5) Source a.k.a. W31C. (6) Complex profile: possible blend of several maser components in velocity interval [−11, 3] km s^{-1}. Definite narrow spike feature (Δv = 0.3 km s^{-1}) at v_{LSR} = − 6.7 km s^{-1}. (7) Two Gaussian emission components were fitted to the data. It is also possible to fit one *emission* and one *absorption* component with $\int S\,dv$ = 63/−27 Jy km s^{-1}, v_{LSR} = 57.2/57.3 km s^{-1}, and Δv = 2.1/0.9 km s^{-1}, where for each quantity the two numbers denote the fit values of the emission and the absorption component, respectively. (8) Possible weak narrow component at v_{LSR} = 6.7 km s^{-1}. Broad emission may be present. (9) Source a.k.a. W75S.

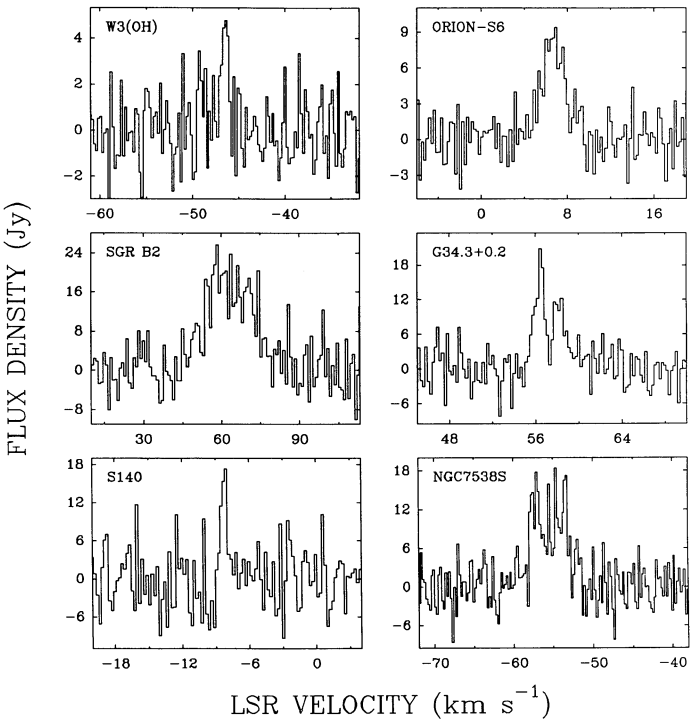

FIG. 3.—Same as Fig. 1, except for the velocity resolution of the spectra, which is 0.89 km s^{-1} for the Sgr B2 spectrum and 0.22 km s^{-1} in all other cases.

TABLE 2

SOURCES WITHOUT DETECTED EMISSION IN THE $7_0 \rightarrow 6_1$ A^+ TRANSITION

Source	α_{1950}	δ_{1950}	v_{LSR} − range (km s^{-1})	ΔS[a] (Jy)
S187 (IRS)	01^{h}19^{m}58^s.0	61°33′08″	[−55, 25]	12
W3 (IRS5)	02 21 53.2	61 52 21	[−80, 0]	13
W3 (Cont)	02 21 56.6	61 52 30	[−90, 0]	12
GL 490	03 23 41.4	58 36 52	[−50, 30]	12
HH 7–11	03 25 58.0	31 05 45	[−30, 50]	13
NGC 2024	05 39 14.0	−01 55 59	[−30, 50]	12
NGC 2071	05 44 30.0	00 20 40	[−10, 30]	17
Mon R2	06 05 22.0	−06 22 25	[−30, 50]	10
G188.94+0.89	06 05 54.0	21 39 09	[−10, 30]	14
IRC+10216	09 45 14.8	13 30 39	[−60, 20]	7
L134N	15 51 32.7	−02 42 51	[−20, 20]	15[b]
Sgr A–G	17 42 27.4	−29 04 36	[−10, 70]	30
G9.62+0.19	18 03 16.0	−20 32 01	[−40, 40]	18
W33B	18 10 59.0	−18 02 39	[20, 100]	33
W33A	18 11 44.5	−17 52 56	[20, 100]	30
G15.04−0.68	18 17 31.6	−16 12 58	[−20, 60]	18
G21.88+0.02	18 28 16.0	−09 51 01	[−20, 60]	18
W43S	18 43 27.0	−02 42 40	[45, 140]	21
G31.29+0.07	18 45 37.0	−01 29 12	[60, 150]	24
W48	18 59 13.8	01 09 13	[0, 90]	16
G43.80−0.13	19 09 31.2	09 30 51	[0, 80]	13
G45.07 + 0.13	19 11 00.3	10 45 45	[10, 90]	23
W51N	19 21 22.4	14 25 13	[20, 90]	22
GL 2591	20 27 36.0	40 01 16	[−25, 20]	30[b]
Cepheus A	22 54 19.0	61 45 47	[−50, 40]	15
NGC 7538 (IR)	23 11 36.7	61 11 49	[−100, −10]	15

[a] 3 σ upper limits on flux density in observed velocity range. The velocity resolution was 0.22 km s^{-1}, except where noted.

[b] Velocity resolution 0.055 km s^{-1}.

likely thermal) emission from the MEC, also intense emission from a narrow spectral feature toward a position that is offset by 10″ from the MEC. Interestingly, the position of the narrow feature (near the infrared source IRc 6) is coincident with the position determined for one of the 25 GHz maser components at the same LSR velocity (8.5 km s^{-1}).

The 44 GHz $7_0 \rightarrow 6_1$ A^+ spectrum observed by us looks remarkably similar to a single dish spectrum of the $8_0 \rightarrow 7_1$ A^+ line (Ohishi *et al.* 1986). In Figure 4 we compare the $7_0 \rightarrow 6_1$ A^+ spectrum with a spectrum of the 36 GHz $4_{-1} \rightarrow 3_0$ E transition. It is obvious that the latter line shows no sign of the very narrow emission feature obvious in the $7_0 \rightarrow 6_1$ A^+ (and the $8_0 \rightarrow 7_1$ A^+) spectra. The $4_{-1} \rightarrow 3_0$ E spectrum has the shape typical of many *thermal* methanol lines observed toward the KL region (Menten *et al.* 1988*c*).

ii) *OMC-2*

In both the 36 and the 44 GHz lines, narrow emission is observed toward the OMC-2 region (Fig. 2), a complex of infrared sources (Gatley *et al.* 1974) about 13′ north of Orion-

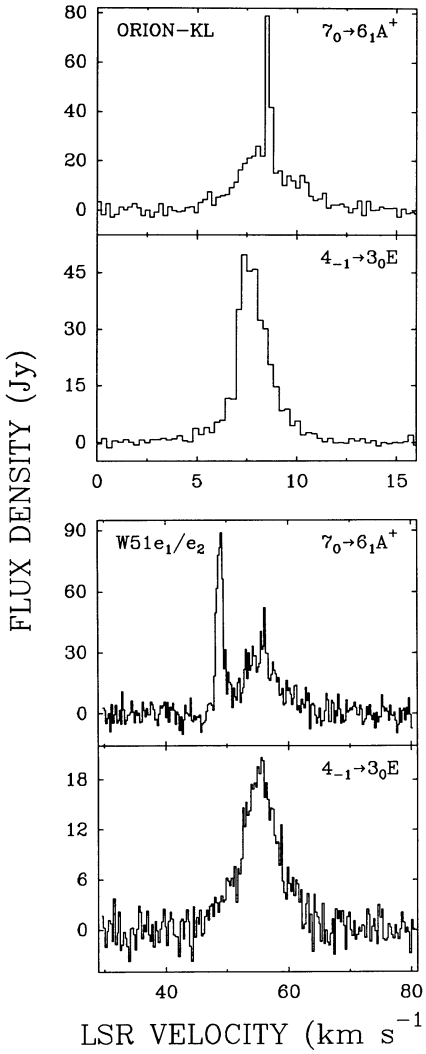

FIG. 4.—Comparison of the $7_0 \rightarrow 6_1$ A^+ and $4_{-1} \rightarrow 3_0$ E spectra observed toward the Orion–KL region and toward a position near the ultracompact H II regions e_1/e_2 in the W51 star-forming region. The velocity resolution is 0.22 km s^{-1} for the $7_0 \rightarrow 6_1$ A^+ spectra and 0.36 km s^{-1} for the $4_{-1} \rightarrow 3_0$ E spectra.

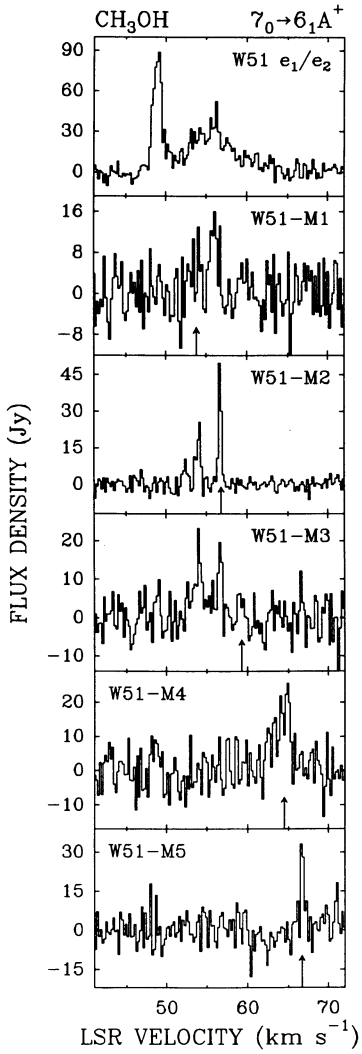

FIG. 5.—$7_0 \rightarrow 6_1$ A^+ spectra taken toward the positions determined by Menten *et al.* (1986*a*) for various masers observed in the 25 GHz $J_2 \rightarrow J_1$ E transitions toward the W51 region (observed positions are listed in Table 1). The velocities of the 25 GHz masers are shown as arrows. The upper panel shows the spectrum toward the e_1/e_2 position (see Fig. 4). All spectra have a velocity resolution of 0.22 km s^{-1}.

KL. In both lines, the velocity is identical to the velocity of the narrow emission found in the $5_2 \rightarrow 5_1$ E and $6_2 \rightarrow 6_1$ E lines by Menten *et al.* (1988*d*). Since all of the four mentioned transitions have line widths of $\Delta v \approx 0.3$–0.4 km s^{-1}, much narrower than the values of ≈ 1.5 km s^{-1} observed for ammonia (Batrla *et al.* 1983) and thermal methanol emission (Menten *et al.* 1988*c*), most likely maser action is observed.

iii) *S235*

Our $7_0 \rightarrow 6_1$ A^+ spectrum (Fig. 2) bears a remarkable resemblance to the spectrum observed in the $8_0 \rightarrow 7_1$ A^+ transition by Nakano and Yoshida (1986). In both transitions, an intense narrow feature ($\Delta v = 0.7$ km s^{-1}) and weaker emission at slightly lower velocities are discernible. The line width of the strong feature is much smaller than the values observed for CO and CS (Nakano and Yoshida 1986) and NH_3 (Ho, Martin, and Barrett 1981), although its velocity is within the range of values observed in the latter species. The $4_{-1} \rightarrow 3_0$ E spectrum also shown in Figure 2 has lower velocity resolution than the

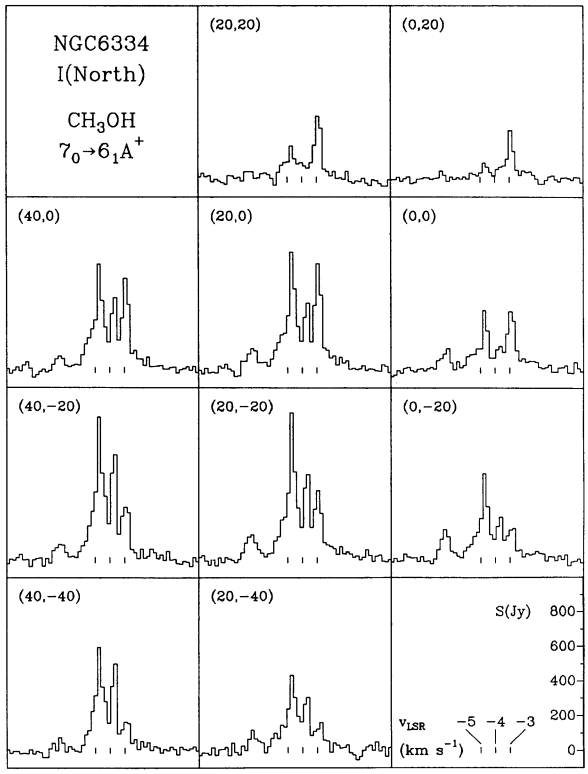

FIG. 6.—Spectra of the $7_0 \rightarrow 6_1$ A^+ transition of CH_3OH taken toward several positions in the NGC 6334-I (North) region. For each spectrum, position offsets (in arcseconds) relative to the position listed in Table 1 are indicated, and the three little marks denote the velocities shown in the *lower right* panel, where the intensity scale is also given. The velocity resolution is 0.22 km s^{-1}.

$7_0 \rightarrow 6_1$ A^+ spectrum, but it is clear that also in this line a narrow component is observed at the velocity of the intense $7_0 \rightarrow 6_1$ $A^+/8_0 \rightarrow 7_1$ A^+ feature, in agreement with the higher resolution $4_{-1} \rightarrow 3_0$ E spectrum presented by Haschick and Baan (1989).

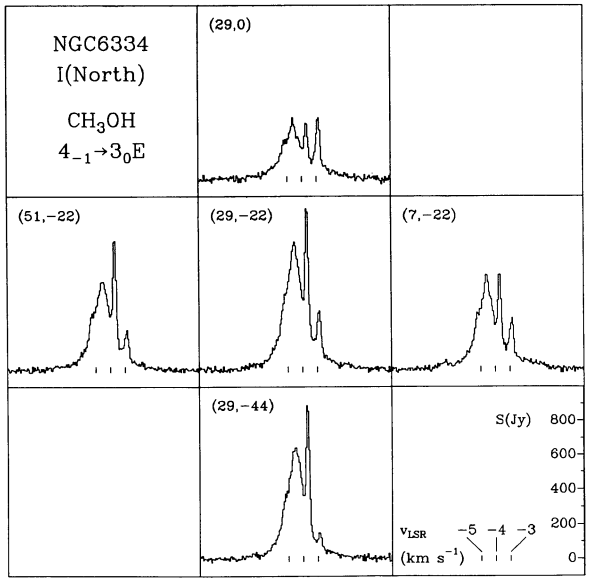

FIG. 7.—Same as Fig. 6, but for the $4_{-1} \rightarrow 3_0$ E line measured at a velocity resolution of 0.067 km s^{-1}.

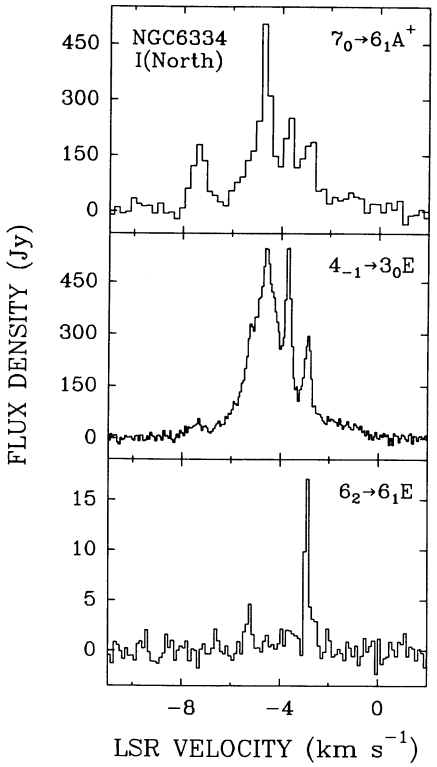

FIG. 8.—A comparison of spectra from three different methanol transitions all taken toward roughly the same position in the NGC 6334-I (North) region. The $7_0 \rightarrow 6_1$ A^+ (*top*) and $4_{-1} \rightarrow 3_0$ E (*middle*) lines are taken from Fig. 6 [(0, −20) offset] and Fig. 7 [(7, −22) offset], respectively. The $6_2 \rightarrow 6_1$ E spectrum is taken from Menten and Batrla (1989) and has a velocity resolution of 0.12 km s^{-1}.

iv) *S255*

The feature detected (Fig. 1) most likely represents maser emission since its line width of 0.6 km s^{-1} is much narrower than typical molecular line widths observed in this region, which are of order 2 km s^{-1} (Evans, Blair, and Beckwith 1977; Ho, Martin and Barrett 1981). We took spectra at offsets of (0, −88″), (0, −44″), (−44″, −44″), and (44″, −44″) relative to the position given in Table 1, but the line was only detected toward the (0, 0) position, indicating that the CH_3OH maser is situated north of the infrared sources IRS 1 and 2 (Beichman, Becklin, and Wynn-Williams 1979) and the H_2O maser (Genzel and Downes 1977). We note that a (sub-)millimeter continuum source has been detected $\approx 1'$ north of IRS 1/2, named S255N by Jaffe *et al.* (1984) and FIR 3 by Mezger *et al.* (1988). Due to insufficient offset measurements, we are unable to determine the position for the methanol maser accurately enough to allow a meaningful comparison with other phenomena in the S255 region.

v) *NGC 2264*

We observe a strong maser feature in the $7_0 \rightarrow 6_1$ A^+ and the $4_{-1} \rightarrow 3_0$ E transitions, at identical velocities, toward the molecular cloud associated with the open cluster NGC 2264 (Fig. 2). The narrow feature in the $4_{-1} \rightarrow 3_0$ E line is spectrally unresolved and appears more clearly in the higher resolution observations of Haschick and Baan (1989). Our offset measurements (Table 3) indicate that the maser is located west of IRS 1 (Allen 1972), the dominant infrared source in the dense cloud core. In addition to the strong maser at $v_{LSR} = 7.2$ km s^{-1}, our high-resolution $7_0 \rightarrow 6_1$ A^+ spectrum also shows possibly narrow emission at slightly higher velocities. In the $4_{-1} \rightarrow 3_0$ E line, in addition to the maser spike, broad emission is observed at velocities comparable to the values observed for emission from CO and NH_3 (Krügel *et al.* 1987) and other methanol lines (Gottlieb *et al.* 1979).

vi) *NGC 6334–I (N)*

This cool (sub-)millimeter continuum source (Gezari 1982) is found about 2′ north of the ultracompact H II region NGC 6334-F (Rodríguez, Cantó, and Moran 1982; Gaume and Mutel 1987). While toward NGC 6334-F all six hitherto known class B methanol maser transitions are detected (Menten and Batrla 1989; Haschick, Baan, and Menten 1989), the northern source I(N), which has no associated centimeter-wave continuum emission (Rodríguez, Cantó, and Moran 1982), is definitively a class A CH_3OH maser source, showing maser emission in the 25 GHz $J_2 \rightarrow J_1$ E lines (Menten and Batrla 1989). As is evident from Figures 6 and 7, I(N) shows spectacularly strong emission in both the 44 GHz $7_0 \rightarrow 6_1$ A^+

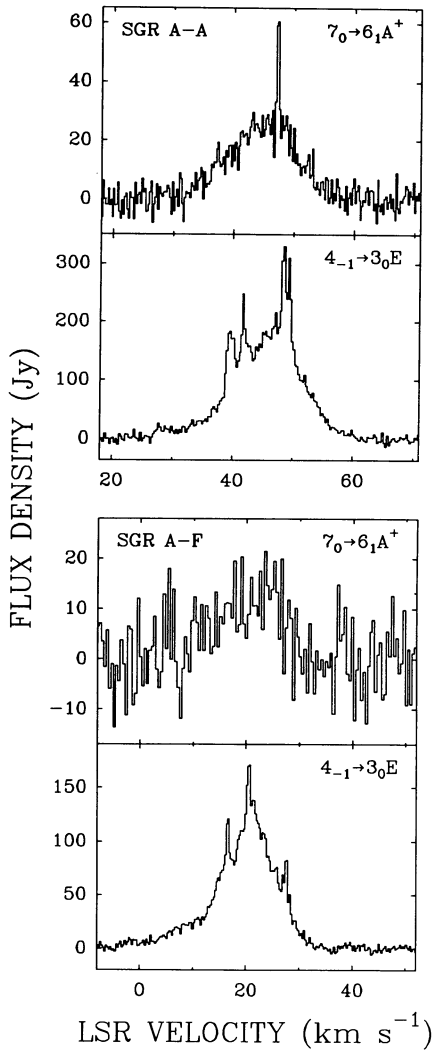

FIG. 9.—Comparison of the $7_0 \rightarrow 6_1$ A^+ and $4_{-1} \rightarrow 3_0$ E spectra observed toward the compact continuum sources Sgr A–A and Sgr A–F in the galactic center region. The velocity resolutions of the $7_0 \rightarrow 6_1$ A^+ spectra are 0.22 km s^{-1} and 0.44 km s^{-1} for Sgr A–A and Sgr A–F, respectively. Both $4_{-1} \rightarrow 3_0$ E spectra have a velocity resolution of 0.36 km s^{-1}.

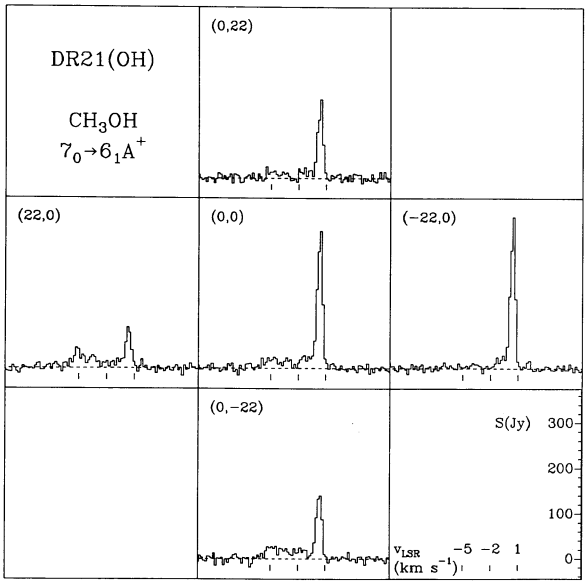

FIG. 10.—Spectra of the $7_0 \rightarrow 6_1$ A^+ transition of CH_3OH taken toward five positions in the DR 21 (OH) region. For each spectrum, position offsets (in arcseconds) relative to the position listed in Table 1 are indicated, and the three little marks denote the velocities shown in the *lower right* panel, where the intensity scale is also given. The velocity resolution is 0.22 km s^{-1}. For each spectrum, the zero level is indicated by the dashed line.

and the 36 GHz $4_{-1} \rightarrow 3_0$ E lines. The $4_{-1} \rightarrow 3_0$ E spectrum looks particularly interesting, since it is a superposition of a number of narrow features and a very intense broad component showing line wings that cover an 8 km s^{-1} velocity interval. Narrow emission features dominate the $7_0 \rightarrow 6_1$ A^+ spectrum, although broad emission may also be present. In Figure 7 we compare the $4_{-1} \rightarrow 3_0$ E, $7_0 \rightarrow 6_1$ A^+, and $6_2 \rightarrow 6_1$ E spectra, all taken toward roughly the same position, and find that two of the narrow components (at $v_{LSR} = -5.2$ and -2.9 km s^{-1}) are definitely seen at identical velocities in all three transitions. The broad emission observed in the $4_{-1} \rightarrow 3_0$ E line will be discussed in more detail in § III*f*.

vii) *Sgr A*

In the $7_0 \rightarrow 6_1$ A^+ transition, we detect a single narrow feature superposed on broad emission toward the compact continuum source Sgr A–A (Ho *et al.* 1985), which is situated 3′ north-east of the galactic center in the molecular cloud M-0.02-0.07, often called the "40 km s^{-1}" cloud (Güsten, Walmsley, and Pauls 1981; Armstrong and Barrett 1985). Only broad emission, but no obvious maser feature, was observed toward the compact continuum source Sgr A–F, 3′ south of the galactic center at the northern end of the "20 km s^{-1}" cloud M-0.13-0.08.

Figure 9 illustrates the remarkably different observational results for $4_{-1} \rightarrow 3_0$ E line on the one hand and the $7_0 \rightarrow 6_1$ A^+ on the other toward the galactic center region: while in the former line intense masers are found over a wide velocity range (superposed on broad emission) toward several positions in the "20 km s^{-1}" cloud (e.g., Sgr A–F) (Haschick and Baan 1989; Szczepanski *et al.* 1989) and in the "40 km s^{-1}" cloud (Sgr A–A), only a single maser feature is observed in the $7_0 \rightarrow 6_1$ A^+ transition toward Sgr A–A and no maser at all and only rather weak broad emission toward Sgr A–F. This asymmetry clearly reflects significant differences in the excitation of both lines.

viii) *G10.6−0.4 (=W31C)*

Menten *et al.* (1986*a*) find spatially compact broad emission in the 25 GHz $J_2 \rightarrow J_1$ E lines near this well-studied compact H II region (Ho and Haschick 1986) and detect two narrow features in these lines at velocities of -8 and -6 km s^{-1} that they find to be offset by $\approx 10''$ in north-eastern direction relative to the continuum source. Due to the insufficient velocity resolution and poor signal-to-noise ratio, it is not possible to decide from our $7_0 \rightarrow 6_1$ A^+ spectrum (Fig. 2) whether narrow features are observed in this line at the velocities of the 25 GHz

TABLE 3

POSITIONS OF $7_0 \rightarrow 6_1$ A^+ MASERS RELATIVE TO KNOWN MASERS IN OTHER CH_3OH TRANSITIONS

SOURCE	OFFSET RELATIVE TO POSITION IN TABLE 1[a]		OFFSET RELATIVE TO OTHER CH_3OH MASER[b]		OTHER CH_3OH MASER LINE	REFERENCE
	$\Delta\alpha$	$\Delta\delta$	$\Delta\alpha$	$\Delta\delta$		
OMC-2	9″(1″)	−2″(1″)	14″(18″)	14″(18″)	$J_2 \rightarrow J_1$ E	1
S235[c]	8 (3)	14 (4)	−1 (16)	20 (17)	$8_0 \rightarrow 7_1$ A^+	2
NGC 2264[d]	−24 (1)	5 (1)	...	...	...	
DR 21–Met	8 (1)	5 (1)	8 (18)	5 (18)	$J_2 \rightarrow J_1$ E	3
DR 21(OH)[e]	−11 (1)	0 (1)	5 (15)	2 (15)	$5_{-1} \rightarrow 4_0$ E	4

[a] Positions were determined by measuring five-point maps with offsets of ±22″ (≈ half the beam size) in right ascension and declination around the positions given in Table 1. Errors given here result from fitting a Gaussian source model to these measurements and *do not* include pointing errors.

[b] Offsets of the $7_0 \rightarrow 6_1$ A^+ masers relative to positions of maser features observed in other CH_3OH lines available in the literature. Errors given are quadratic sums of the formal errors of the $7_0 \rightarrow 6_1$ A^+ position determination (see above), uncertainties in the position of the maser in the other line (as given in the respective reference) and, dominating, the estimated pointing error of our observations (15″).

[c] $8_0 \rightarrow 7_1$ A^+ position determined from Fig. 3b of Nakano and Yoshida 1986. A pointing error of 5″ was assumed.

[d] No accurate position is available for the CH_3OH maser observed in the $4_{-1} \rightarrow 3_0$ E transition shown in Fig. 2 and first reported by Haschick and Baan 1989.

[e] Positions refer to the strongest spectral feature ($v_{LSR} = 0.4$ km s^{-1}). The $5_{-1} \rightarrow 4_0$ E position (Nakano and Yoshida 1986) was determined by interferometric measurements.

REFERENCES.—(1) Menten *et al.* 1988*b*; (2) Nakano and Yoshida 1986; (3) Menten *et al.* 1986*a*; (4) Batrla and Menten 1988.

masers, although emission is present in this velocity range and *not* between -4 and 4 km s^{-1}, where the broad 25 GHz emission is observed. One definite narrow feature is observed at $v_{LSR} \approx -7$ km s^{-1}. In contrast, the $4_{-1} \rightarrow 3_0$ E transition clearly shows a narrow feature at -6 km s^{-1} (see also Haschick and Baan 1989).

ix) *W33-Met*

This position, $\approx 40''$ west of the compact continuum source W33 Main (Haschick and Ho 1983), was determined by Menten *et al.* (1986*a*) as the location of a narrow spike feature observed in the 25 GHz $J_2 \rightarrow J_1$ E lines at a velocity of 33 km s^{-1}. We find an intense narrow feature at the same velocity and additional emission at higher velocities, which may be a blend of additional narrow features or broad emission. Broad emission is also observed in the low J ($J = 2, 3, 4$) $J_2 \rightarrow J_1$ E lines (Menten *et al.* 1986*a*).

x) *G30.8−0.1*

Not many molecular line observations have been conducted toward the G30.8−0.0 H II region association, which is within the W43 complex. We observed the position of the water maser W43 Main (3) in the nomenclature of Genzel and Downes (1977) and detected strong emission in the $4_{-1} \rightarrow 3_0$ E (see also Haschick and Baan 1989) and the $7_0 \rightarrow 6_1$ A^+ transitions (Fig. 2). Both lines show complex velocity structure not discernible in the lower resolution spectrum of the $7_0 \rightarrow 6_1$ A^+ transition presented by Morimoto, Ohishi, and Kanzawa (1985). No very narrow features seem to be present, although one component in the $7_0 \rightarrow 6_1$ A^+ spectrum has a line width of 0.9 km s^{-1}. Unfortunately no offset measurements are available to determine the position of the CH_3OH emission relative to the H_2O maser and the infrared and radio sources (Lester *et al.* 1985) in this interesting region.

xi) *The Sources in the W51 Region*

Hot compact molecular cores have been detected near the ultracompact H II regions e_1/e_2 and d in the distant W51 star-forming region. Detailed studies of NH_3 (Ho, Genzel, and Das 1983; Mauersberger *et al.* 1985; Mauersberger, Henkel, and Wilson 1987), OH (Gaume and Mutel 1987) and H_2O (Schneps *et al.* 1981) have been conducted in the past. (Note that the H_2O maser centers W51 South, W51 Main, and W51 North are close to the H II regions e_1, e_2, and d, respectively. W51 d is associated with the infrared source W51 IRS 2.) Menten *et al.* (1986*a*) observed strong thermal emission in the 25 GHz $J_2 \rightarrow J_1$ E lines of CH_3OH toward e_1/e_2 for which they derived a rotation temperature of ≈ 100 K and weaker extended emission. They also detected maser emission in the 25 GHz lines toward five different positions spread over an area of $2' \times 2'$ ($2'$ corresponds to 4.7 pc at the 8 kpc distance of W51). Each of the maser components is separated by at least $50''$ (1.9 pc) from the nearest known compact H II region (either e_1, e_2, or d).

The $7_0 \rightarrow 6_1$ A^+ transition was first observed toward W51 by Morimoto, Ohishi, and Kanzawa (1985). Their spectrum closely resembles our spectrum taken toward the e_1/e_2 position (Fig. 4), showing broad emission between velocities of 45 and 65 km s^{-1} and an intense narrower feature at a velocity of 49 km s^{-1}. While the broad component closely resembles the nonmaser spectra observed in other molecules (Ho, Genzel, and Das 1983; Mauersberger *et al.* 1985; Mauersberger, Henkel, and Wilson 1987) and a number of methanol transitions (Menten *et al.* 1986*a*; Haschick and Baan 1989; see also Fig. 4), the narrow component has no equivalent in any other line. We note that the 49 km s^{-1} feature is significantly broader ($\Delta v = 1.2$ km s^{-1}) than "typical" narrow features.

We also detect, most interestingly, narrow emission in the $7_0 \rightarrow 6_1$ A^+ line toward all the 25 GHz maser positions determined by Menten *et al.* (1986*a*) (see their Table 4). Moreover, from Figure 5 we see that the $7_0 \rightarrow 6_1$ A^+ masers also have velocities (marked by the arrows) identical to the velocities of the respective 25 GHz maser components. Since the W51-Met1, -Met2, and -Met3 positions are separated by less than one beamwidth, one and the same feature may appear in more than one spectrum. The fact that the Met1 maser appears stronger on the nearby Met2 and Met3 positions is easily explainable by the pointing uncertainties of our observations. We do not clearly detect the third maser in the list of Menten *et al.*, but we note that this is the weakest component reported by these authors.

xii) *DR 21–West*

The maser found in the 25 GHz $J_2 \rightarrow J_1$ E lines toward the DR 21 region by Menten *et al.* (1986*a*) represents one of the most clear-cut examples of the fact that 25 GHz CH_3OH masers are frequently detected offset from known radio-continuum, infrared, and other molecular (OH and H_2O) maser sources. In this case, the 25 GHz maser is found to be offset by $\approx 75''$ (= 1.1 pc) from the nearest known IR source. We detect strong emission in both the $4_{-1} \rightarrow 3_0$ E and the $7_0 \rightarrow 6_1$ A^+ transitions toward the position determined by Menten *et al.* (1986*a*) at the same velocity as the $J_2 \rightarrow J_1$ E maser. In contrast, toward the canonical DR 21 infrared/radio-continuum position, only thermal emission is detected in the 25 GHz lines (Menten *et al.* 1986*a*) and in the $7_0 \rightarrow 6_1$ A^+ transitions (Table 2) and no emission is detected in the $4_{-1} \rightarrow 3_0$ E line (Haschick and Baan 1989).

xiii) *DR 21*(OH)(= *W75S*)

Toward this source, both the 36 GHz $4_{-1} \rightarrow 3_0$ E (Haschick and Baan 1989) and the 44 GHz $7_0 \rightarrow 6_1$ A^+ spectra (Fig. 1) look very similar to the spectrum of the $5_{-1} \rightarrow 4_0$ E transition at 84 GHz (Menten *et al.* 1989), showing a strong narrow feature at a velocity of 0.4 km s^{-1} and a broad component at lower velocities. Batrla and Menten (1988) used the Hat Creek interferometer to map the $5_{-1} \rightarrow 4_0$ E emission at $\approx 7''$ resolution and found the strong component to be a blend of two features both offset in western direction from the known centers of activity in the region as marked by OH and H_2O masers, and the H_2CO emission peaks. The CH_3OH masers are also offset from the compact $C^{18}O$ $J = 2 \rightarrow 1$ and 1.4 mm continuum emission distributions mapped by Padin *et al.* (1989) and Woody *et al.* (1989) with $3''$ resolution, although we note that the strongest $5_{-1} \rightarrow 4_0$ E maser feature is located outside the field of view determined by the primary beam position of the latter two interferometric studies. Batrla and Menten found the broad emission to be a superposition of a number of narrower features spread over an area of $30'' \times 50''$, comparable to our beam size. Our five-point map (measured at half-beam spacing) in the $7_0 \rightarrow 6_1$ A^+ line (Fig. 10) is consistent with the spatial distribution found in the $5_{-1} \rightarrow 4_0$ E transition and within the pointing uncertainties the position of the 0.4 km s^{-1} features are identical for both lines. We note that only thermal and *no maser* emission was observed by Menten *et al.* (1986*a*) in the $J_2 \rightarrow J_1$ E lines.

c) *The $7_0 \rightarrow 6_1$ A^+ Masers*

There are several facts that indicate that the narrow features observed in the spectra of many of the sources in our sample represent maser emission:

1. Their line widths are of order 0.2–0.7 km s^{-1}, much smaller than typical molecular line widths in the regions in question.

2. Toward a number of sources showing strong narrow features, we have performed offset measurements (five-point maps with half-beam spacing) around several of the positions given in Table 1 (see Table 3). We find that the emission regions are pointlike relative to our 46″ beam at 44 GHz, implying upper limits of 23″ to their sizes. From these upper limits we calculate lower limits to their brightness temperatures of greater than 350 K for OMC-2, NGC 2264, NGC 6334–I(N), DR 21–West, and DR 21 (OH). These values are greater than any estimate for the kinetic temperature of the molecular gas in these regions.

3. As mentioned, in a number of sources, spectral appearance and spatial distribution of the narrow emission observed in the $7_0 \rightarrow 6_1$ A^+ and/or the $4_{-1} \rightarrow 3_0$ E transition closely resembles the properties of CH_3OH maser emission from other transitions observed toward the same regions. The existence of masers in any transition points to the fact that special conditions are present in the sources in question that may also favor inversion of other lines. The connection between CH_3OH masers from different transitions will be discussed in the next section.

The spectra of the methanol masers observed by us look distinctly different from OH and H_2O maser spectra observed toward the same regions: many more velocity components are present in spectra from the latter species. Moreover, the methanol spectra show no signs of the high-velocity features that are present in H_2O spectra toward many of the sources (Genzel and Downes 1977).

d) *The Relation among 25, 36, 44, 84, and 95* GHz *Methanol Masers*

In cases where maser emission is observed from various transitions of one and the same molecule, one might hope that multitransition studies would yield interesting information about the pumping mechanisms involved and, ultimately, about the physical conditions prevailing in the regions from which the masers arise.

Methanol masers are especially interesting in this respect, since many maser transitions have been found from states with widely differing excitation energies. It has been recognized that methanol sources masing in the $2_0 \rightarrow 3_{-1}$ E transition at 12 GHz are distinctly different from sources masing in the 25 GHz $J_2 \rightarrow J_1$ E lines. Batrla *et al.* (1987) designated the latter sources as class A and the 12 GHz maser sources as class B methanol masers. To summarize, class B masers, which have the ultracompact H II region W3(OH) as their prototype, are found close to OH masers associated with ultracompact H II regions. Class A masers, in contrast, are not associated with masers from other molecular species, compact continuum sources, or infrared objects. Toward Orion-KL, the prototypical class A source, individual maser components are spread over a 30″ × 40″ (=0.07 pc × 0.09 pc) area that is clearly offset from the well-studied IR and OH or H_2O maser sources (Matsakis *et al.* 1980). On the other hand, VLBI results for the W3(OH) 12 GHz masers show that they are clustered on a 100 times smaller size scale and are projected on the compact continuum source in the same region as the OH masers (Menten *et al.* 1988*b*).

Several other CH_3OH maser transitions were observed toward W3(OH) with spectra and spatial distributions similar to the 12 GHz line and were accordingly classified as class B transitions (Batrla *et al.* 1987; Menten *et al.* 1988*a*; Haschick, Baan, and Menten 1989).

However, a number of other transitions at 36, 44, 84, and 95 GHz were also found to show evidence for maser action [notably *not* toward W3(OH)] and seemed, on first look, difficult to classify. As described in § III*b*, toward many regions spectra observed in two or more of these transitions look very similar. Also the spatial distributions observed in different transitions seem to be comparable. Taking all this evidence together leads us to believe that the known masers in the 36 GHz $4_{-1} \rightarrow 3_0$ E, the 84 GHz $5_{-1} \rightarrow 4_0$ E, the 44 GHz $7_0 \rightarrow 6_1$ A^+, and the 95 GHz $8_0 \rightarrow 7_1$ A^+ transitions have many characteristics in common and, in a number of regions, show the same characteristics as the 25 GHz masers. Consequently, all sources showing maser emission in any of these transitions should be categorized as class A methanol masers. There are in fact regions that give rise to maser emission in *all* the lines listed above and, most remarkably, with virtually identical spectral appearance in all these lines (examples: OMC-2 and DR 21). Furthermore, we think that the fact that most of the regions do not show maser action in all, but only some, of the mentioned lines [e.g., Orion-KL, DR 21 (OH)] reflects differences in the physical conditions between these different regions.

e) *The Excitation of Class A Methanol Masers*

Statistical equilibrium calculations performed by Morimoto, Ohishi, and Kanzawa (1985), Ohishi (1984), and Walmsley *et al.* (1988, and personal communication) show that population inversion for the $4_{-1} \rightarrow 3_0$ E, $5_{-1} \rightarrow 4_0$ E, $7_0 \rightarrow 6_1$ A^+, and the $8_0 \rightarrow 7_1 A^+$ transitions can be achieved over a range of excitation conditions. Depending on the choice of the model input parameters for the kinetic temperature, the H_2 density, and the methanol abundance, and using a large-velocity gradient model to calculate the radiative transfer, one or more of the four transitions is found to be inverted. In fact, the observed pattern of maser or nonmaser emission in the individual lines may be used to yield at least order of magnitude estimates of the densities in the masing regions.

The fact that the mentioned lines are masing can, at least qualitatively, be understood by some simple arguments that have been brought forward to explain the $4_{-1} \rightarrow 3_0$ E and $5_{-1} \rightarrow 4_0$ E masers and the enhanced absorption observed in the $2_0 \rightarrow 3_{-1}$ E line toward a number of sources (Lees 1973; Walmsley *et al.* 1988): It is easy to overpopulate the lower levels of the $k = -1$ ladder of E-type methanol because molecules collisionally excited into levels with high J and k quantum numbers rapidly decay via spontaneous transitions into various J levels of the $k = -1$ ladder. Because of the fact that collisions strongly prefer $\Delta k = 0$ transitions, once the molecules are in the $k = -1$ ladder they decay down this ladder to overpopulate the lower $k = -1$ levels, giving rise to the $4_{-1} \rightarrow 3_0$ E and $5_{-1} \rightarrow 4_0$ E masers and enhanced absorption in the $2_0 \rightarrow 3_{-1}$ E line.

For A-type methanol the situation is analogous, only in this case the levels of the $K = 0$ ladder are the endpoints of the

spontaneous decay routes, resulting in the $7_0 \rightarrow 6_1\ A^+$ and $8_0 \rightarrow 7_1\ A^+$ masers.

We note that the mentioned statistical equilibrium calculations do not straightforwardly yield inversion of the $J_2 \rightarrow J_1$ E transitions (Walmsley, personal communication). However, the observational evidence presented in § III*b* indicates that the $J_2 \rightarrow J_1$ E masers emerge from the same regions as the other class A maser lines.

f) *Properties of the Broad Thermal Emission*

Thermal (nonmaser) emission from many methanol lines in the centimeter- and millimeter-wave range has been observed toward numerous dense molecular cloud cores associated with star-forming regions (Gottlieb *et al.* 1979; Menten *et al.* 1986*a*, *b*). Menten *et al.* (1986*a*, *b*, 1988*c*) find enhanced methanol abundances of $[CH_3OH/H_2] = 10^{-7}$ to 10^{-6} in hot regions, two to three orders of magnitude higher than predicted by gas-phase chemical models, and they argue that evaporation of methanol molecules from grain mantles may cause such high abundances.

Although many hot molecular cores are in our sample, we detect broad thermal emission in the $7_0 \rightarrow 6_1\ A^+$ transition only toward a small number of sources. This is easily understandable in view of the limited sensitivity of our observations. One should also keep in mind that the excitation energy above the ground state E_u/k is 65 K for the $7_0\ A^+$ level. The warm molecular gas with temperatures that are high enough to significantly populate energy levels at such excitation energies is confined to compact regions close to the embedded heating sources. For distant galactic sources, the resulting emission is heavily diluted in our 46″ beam. On the other hand, because of its much lower excitation energy ($E_u/k = 21$ K), the $4_{-1} \rightarrow 3_0\ E$ line is excited over larger volumes, and thermal emission in this line is easier to observe (see Haschick and Baan 1989).

To put things more quantitatively, we use the equations given by Menten *et al.* (1986*a*) and, assuming optically thin emission, derive the following relation between the total methanol column density $\mathcal{N}(CH_3OH)$ in cm^{-2} and the observed integrated antenna temperature $\int T_A^* dv$ in K km s^{-1}:

$$\int T_A^* dv = 6.0 \times 10^{-15} f \eta_M \nu \mu^2 S \times \frac{\mathcal{N}(CH_3OH)}{Q} \exp\left(-\frac{E_u}{kT_{rot}}\right), \quad (1)$$

where η_M is the main-beam efficiency. The beam filling factor f is given by $f = \theta_s^2/(\theta_s^2 + \theta_b^2)$ assuming Gaussian beam and source distributions with half-widths θ_b^2 and θ_s^2, respectively. S is the line strength and ν and μ denote the line frequency in GHz and the magnetic dipole moment in D, respectively; $\mu = 1.412$ D for b-type ($\Delta k = \pm 1$) transitions. Q, the methanol partition function, is well approximated by the expression

$$Q = 2 \times 0.64 T_{rot}^{1.5}, \quad (2)$$

in which the factor 2 expresses the fact that (at not too low temperatures) equal amounts of methanol are in the E and A symmetry species. T_{rot} is the rotation temperature in K, k is the Boltzmann constant, and E_u is the energy of the upper energy level relative to the 1_{-1} level for E-type lines and relative to the 0_0 level for A-type lines. Plugging in all the numbers, we obtain

$$\int T_A^* dv(\text{K km s}^{-1}) = \mathscr{C} f \mathcal{N}(CH_3OH)(\text{cm}^{-2}) \times \frac{\exp\left[-E_u/(kT_{rot})\right]}{T_{rot}^{1.5}}, \quad (3)$$

where the factor $\mathscr{C}$ is equal to 1.3×10^{-13} for the $7_0 \rightarrow 6_1\ A^+$ line and 6.7×10^{-14} for the $4_{-1} \rightarrow 3_0\ E$ line.

Since the main objective of the observations reported in this article was a search for masers in the $7_0 \rightarrow 6_1\ A^+$ transition, the integration times spent on most sources were not long enough to allow meaningful studies of the thermal emission component, if present. Therefore we restrict our discussion to a few sources of special interest.

i) *Orion-KL and S6*

Nonmaser methanol lines observed toward the KL region usually can be decomposed in a narrow ($\Delta v \approx 2.2$ km s^{-1}) component at an LSR velocity of 8 km s^{-1} and a broad ($\Delta v \approx 6.5$ km s^{-1}, $v_{LSR} \approx 6.5$ km s^{-1}) component (see, for example, the $4_{-1} \rightarrow 3_0\ E$ spectrum in Fig. 4). It is difficult to tell what portion of our $7_0 \rightarrow 6_1\ A^+$ spectrum represents maser emission in addition to the narrow maser spike observed at 8.57 km s^{-1}. Certainly the profile has some emission at velocities higher than the spike velocity that is not well fit by the canonical two components described above. This is more obvious in the higher quality $7_0 \rightarrow 6_1\ A^+$ spectrum presented by Ohishi (1984). If we use the methanol column densities and rotation temperatures calculated by Menten *et al.* (1988*c*) and assume an extent of 15″ for both thermal emission components (Wilson *et al.* 1989), we predict a total integrated antenna temperature of 3 K for the thermal $7_0 \rightarrow 6_1\ A^+$ emission that is, within the uncertainties, consistent with the 2.5 K measured by us. (We note that, because of the low signal-to-noise ratio of the spectrum, we fitted only one broad Gaussian to the thermal emission and one very narrow Gaussian to the strong maser spike at 8.57 km s^{-1}.)

Methanol observations toward the ammonia peak Source 6 (S6) in the notation of Batrla *et al.* (1983), a strong molecular and (sub-)millimeter continuum source about 2′ south of the KL-region, have previously been reported by Menten *et al.* (1988*c*) and Haschick and Baan (1989). Using $T_{rot} = 79$ K and $\mathcal{N}(CH_3OH) = 3.2 \times 10^{16}$ (Menten *et al.* 1988*a*) and assuming a source size of 30″, we calculate an expected value of $\int T_A^* dv = 0.8$ K km s^{-1} for the $7_0 \rightarrow 6_1\ A^+$ line, in excellent agreement with the measured 0.7 K km s^{-1}.

ii) *Sgr A*

It is difficult to estimate CH_3OH column densities and rotation temperatures from hitherto observed methanol lines toward the Sgr A region: a major contribution to the observed $4_{-1} \rightarrow 3_0\ E$ intensities certainly is maser emission (Haschick and Baan 1989; Szczepanski *et al.* 1989), and the $2_0 \rightarrow 3_{-1}\ E$ line shows in both the ^{12}C and the ^{13}C isotopes (possibly enhanced) absorption toward both the 20 km s^{-1} and the 40 km s^{-1} clouds (Kuiper *et al.* 1989). From observations of the 25 GHz $2_2 \rightarrow 2_1\ E$, $3_2 \rightarrow 3_1\ E$, and $4_2 \rightarrow 4_1\ E$ transitions (Menten *et al.* 1986*a*) toward a position about 40″ south of Sgr A–G, one estimates $T_{rot} \approx 20$ K and $\mathcal{N}(CH_3OH) \approx 6 \times 10^{15}$ cm^{-2}. Due to the uncertainties in the $J_2 \rightarrow J_1\ E$ measurements, these values should not be taken too seriously. Ammonia measurements give values for the NH_3 rotation temperature between 50 and 100 K (Güsten *et al.* 1981, 1985; Mauersberger *et al.* 1986), and dissipation of kinetic energy has been forwarded as a feasible heating mechanism. If we assume 50 K and 5×10^{15} cm^{-2} for the methanol rotation temperature and column density, respectively, and assume a smooth distribution of methanol throughout the 20 km s^{-1} cloud (which includes both the Sgr A–F and G positions), we calculate an integrated intensity of 0.5 K km s^{-1} for the $7_0 \rightarrow 6_1\ A^+$ line. This number is in agreement with the upper limit we obtained

toward Sgr A–G but one order of magnitude lower than the weak detection toward Sgr A–F. For the $4_{-1} \rightarrow 3_0$ E we calculate $\int T_A^* \, dv = 0.6$ K km s^{-1}. This rather small number makes it likely that most of the observed emission in the $4_{-1} \rightarrow 3_0$ E line (Haschick and Baan 1989; Szczepanski *et al.* 1989; see also Fig. 9) is due to maser action.

iii) *NGC 6334–I(N)*

Although no clear sign of broad emission is seen in the $7_0 \rightarrow 6_1$ A^+ transition, a spectacular strong broad feature shows up in the $4_{-1} \rightarrow 3_0$ E line (Fig. 7). Moreover, the $4_{-1} \rightarrow 3_0$ E spectra look quite complicated and show evidence for at least seven different velocity components (as identified in Fig. 8), some of which have, as mentioned in § III*b*, counterparts in the $7_0 \rightarrow 6_1$ A^+ and $J_2 \rightarrow J_1$ E transitions. To analyze the $4_{-1} \rightarrow 3_0$ E emission in more detail, we have fitted five Gaussian velocity components to the spectra measured toward different offset positions (see Fig. 7). Components 1 and 2 (Fig. 8) have not been fitted, since they do not clearly show up at all the observed positions. For each component, the fit results toward the five offset positions have been fitted by a Gaussian source model with offsets in right ascension, declination, integrated intensity at peak position, and half-power source width (assumed to be equal in both coordinates) as free parameters. The results of these fits together with the measured line widths and LSR velocities of the individual components are presented in Table 4. It is obvious that only the broad ($\Delta v = 4.2$ km s^{-1}) component (number 7 in Table 4/Fig. 7) at $v_{\rm LSR} = -4.2$ km s^{-1} appears significantly extended in our 56″ beam, having a "deconvolved" source size θ_s [$= (\theta^2 - \theta_b^2)^{1/2}$] of $33'' < \theta_s < 69''$. The *thermal* emission from the $J_2 \rightarrow J_1$ E lines observed by Menten and Batrla (1989) toward NGC 6334–I(N) has a line width and LSR velocity similar to the values determined for the broad component of the $4_{-1} \rightarrow 3_0$ E emission. However, if we use the methanol column densities and rotation temperature Menten and Batrla derived from their $J_2 \rightarrow J_1$ E measurements, we calculate an expected integrated intensity for the broad component in the $4_{-1} \rightarrow 3_0$ E transition that is too low by an order of magnitude. We speculate that the $4_{-1} \rightarrow 3_0$ E line may be inverted over a large volume giving rise to spatially extended strong emission.

IV. SUMMARY

We have detected emission from the $7_0 \rightarrow 6_1$ A^+ transition of interstellar methanol at 44 GHz toward 25 galactic star-forming regions. A number of sources were also observed in the $4_{-1} \rightarrow 3_0$ E transition at 36 GHz. Toward 16 sources, unambiguously narrow emission components are detected with line widths less than 1 km s^{-1}, much smaller than typical molecular line widths in these regions. These narrow components almost certainly represent maser emission.

The $7_0 \rightarrow 6_1$ A^+ and $4_{-1} \rightarrow 3_0$ E spectra typically show one or only a few narrow features in a small-velocity interval and are thus very different from OH and H_2O maser spectra observed toward the same regions. Masers in the latter species usually show many more components. No high-velocity components are observed in the methanol spectra.

To analyze the spatial distribution of the methanol emission, the $7_0 \rightarrow 6_1$ A^+ line was mapped in a number of sources. In most cases where multiple narrow spectral components are detected, the individual features are found to emerge from different locations. In some sources, the distances between different maser components are of order 1 pc, much larger than typical separations between individual components in OH or H_2O maser clusters. Furthermore, unlike the well-studied 12 GHz methanol masers, the $7_0 \rightarrow 6_1$ A^+ masers appear well separated from OH/H_2O maser centers and compact H II regions and thus show the same behavior as the masers detected in the series of $J_{k=2} \rightarrow J_{k=1}$ E transitions at around 25 GHz. Moreover, spectra of the 44 and 25 GHz transitions resemble each other perfectly in many cases. Also, narrow components identified in $7_0 \rightarrow 6_1$ A^+ spectra have counterparts at the same velocity in the $8_0 \rightarrow 7_1$ A^+, $4_{-1} \rightarrow 3_0$ E, and $5_{-1} \rightarrow 4_0$ E transitions at 95, 36, and 84 GHz, respectively. The simultaneous occurrence of maser emission in the latter four transitions can be understood on the basis of statistical equilibrium calculations.

Toward a number of sources (e.g., Orion, Sgr A), thermal emission is detected at the intensities expected from values of the methanol rotation temperature and column density derived from other transitions. Thermal emission is usually more prominent in the lower excitation $4_{-1} \rightarrow 3_0$ E line. Toward the cool dust continuum source NGC 6334–I(N), in

TABLE 4

EMISSION COMPONENTS OBSERVED IN THE $4_{-1} \rightarrow 3_0$ E LINE TOWARD NGC 6334–I(N)

Component Number	$\int S \, dv$[a] (K km s^{-1})	$v_{\rm LSR}$ (km s^{-1})	Δv (km s^{-1})	$\Delta\alpha$[b]	$\Delta\delta$[b]	θ[b]
1[c]	~50	−7.5 (0.1)	0.5(0.1)	...[d]	...[d]	...[d]
2[e]	~20	−5.25(0.02)	~0.2	...[d]	...[d]	...[d]
3[c]	79(8)	−4.53(0.03)	0.4(0.1)	31″(2″)	−35″(4″)	47″(5″)
4[c]	187(3)	−3.70(0.01)	0.22(0.01)	34 (1)	−35 (1)	55 (2)
5[c,e]	90(4)	−2.89(0.01)	0.30(0.03)	23 (2)	−53 (3)	59 (4)
6	870(30)	−4.60(0.02)	1.5(0.1)	29 (1)	−31 (1)	51 (3)
7	510(30)	−4.2 (0.1)	4.2(0.3)	15 (3)	−15 (3)	77 (12)

[a] Integrated flux density at peak position.

[b] $\Delta\alpha$ and $\Delta\delta$ denote right ascension and declination offset relative to the position listed in Table 1, as determined from fitting a Gaussian source model to our offset measurements. θ gives the half-power width of the Gaussian convolved with the 56″ HPBW of the 37 m telescope. The given uncertainties are formal errors from the fit and do not include pointing errors, which should be smaller than 15″.

[c] Narrow component at this velocity in spectrum of $7_0 \rightarrow 6_1$ A^+ transition (see Fig. 8).

[d] Position of this component could not be determined due to limited signal-to-noise ratio.

[e] Narrow component at this velocity in spectra of $J_2 \rightarrow J_1$ E transitions (see Fig. 8).

addition to intense narrow emission, anomalously strong broad emission is observed that appears to be spatially extended.

We would like to thank C. M. Walmsley and the referee, R. L. Plambeck, for useful comments on this paper.

REFERENCES

Allen, D. 1972, *Ap. J.* (*Letters*), **172**, L55.
Armstrong, J. T., and Barrett, A. H. 1985, *Ap. J. Suppl.*, **57**, 535.
Barrett, A. H., Schwartz, P. R., and Waters, J. W. 1971, *Ap. J.* (*Letters*), **168**, L101.
Batrla, W., Matthews, H. E., Menten, K. M., and Walmsley, C. M. 1987, *Nature*, **326**, 49.
Batrla, W., and Menten, K. M. 1988, *Ap. J.* (*Letters*), **329**, L117.
Batrla, W., Wilson, T. L., Bastien, P., and Ruf, K. 1983, *Astr. Ap.*, **128**, 279.
Beichman, C. A., Becklin, E. E., and Wynn-Williams, C. G. 1979, *Ap. J.* (*Letters*), **232**, L47.
Evans, N. J., II, Blair, G. N., and Beckwith, S. 1977, *Ap. J.*, **217**, 448.
Gatley, I., Becklin, E. E., Matthews, K., Neugebauer, G., Penston, M. V., and Scoville, N. Z. 1974, *Ap. J.* (*Letters*), **191**, L121.
Gaume, R. A., and Mutel, R. L. 1987, *Ap. J. Suppl.*, **65**, 193.
Genzel, R., and Downes, D. 1977, *Astr. Ap. Suppl.*, **30**, 145.
Gezari, D. Y. 1982, *Ap. J.* (*Letters*), **259**, L29.
Gottlieb, C. A., Ball, J. A., Gottlieb, E. W., and Dickinson, D. F. 1979, *Ap. J.*, **227**, 422.
Güsten, R., Walmsley, C. M., and Pauls, T. 1981, *Astr. Ap.*, **103**, 197.
Güsten, R., Walmsley, C. M., Ungerechts, H., and Chuchwell, E. 1985, *Astr. Ap.*, **142**, 381.
Haschick, A. D., and Baan, W. A. 1989, *Ap. J.*, **339**, 949.
Haschick, A. D., Baan, W. A., and Menten, K. M. 1989, *Ap. J.*, **346**, 330.
Haschick, A. D., and Ho, P. T. P. 1983, *Ap. J.*, **267**, 638.
Ho, P. T. P., Genzel, R., and Das, A. 1983, *Ap. J.*, **266**, 596.
Ho, P. T. P., and Haschick, A. D. 1986, *Ap. J.*, **304**, 501.
Ho, P. T. P., Jackson, J. M., Barrett, A. H., and Armstrong, J. T. 1985, *Ap. J.*, **288**, 375.
Ho, P. T. P., Martin, R. N., and Barrett, A. H. 1981, *Ap. J.*, **246**, 761.
Jaffe, D. T., Davidson, J. A., Dragovan, M., and Hildebrand, R. H. 1984, *Ap. J.*, **284**, 637.
Krügel, E., Güsten, R., Schulz, A., and Thum, C. 1987, *Astr. Ap.*, **185**, 283.
Kuiper, T. B. H., Peters, W. L., III, Gardner, F. F., Whiteoak, J. B., and Reynolds, J. E. 1989, *Ap. J.* (*Letters*), **340**, L41.
Lees, R. M. 1973, *Ap. J.*, **184**, 763.
Lester, D. F., Dinerstein, H. L., Werner, M. W., Harvey, P. M., Evans, N. J., II, and Brown, R. L. 1985, *Ap. J.*, **296**, 565.
Matsakis, D. N., Cheung, A. C., Wright, M. C. H., Askne, J. I. H., Townes, C. H., and Welch, W. J. 1980, *Ap. J.*, **236**, 481.
Mauersberger, R., Henkel, C., and Wilson, T. L. 1987, *Astr. Ap.*, **173**, 352.
Mauersberger, R., Henkel, C., Wilson, T. L., and Walmsley, C. M. 1986, *Astr. Ap.*, **162**, 199.
Mauersberger, R., Wilson, T. L., Batrla, W., Walmsley, C. M., and Henkel, C. 1985, *Astr. Ap.*, **146**, 168.
Menten, K. M., and Batrla, W. 1989, *Ap. J.*, **341**, 839.
Menten, K. M., Johnston, K. J., Wadiak, E. J., Walmsley, C. M., and Wilson, T. L. 1988*a*, *Ap. J.* (*Letters*), **331**, L41.
Menten, K. M., Reid, M. J., Moran, J. M., Wilson, T. L., Johnston, K. J., and Batrla, W. 1988*b*, *Ap. J.* (*Letters*), **333**, L83.
Menten, K. M., Walmsley, C. M., Henkel, C., and Wilson, T. L. 1986*a*, *Astr. Ap.*, **157**, 318.
———. 1988*c*, *Astr. Ap.*, **198**, 253.
———. 1988*d*, *Astr. Ap.*, **198**, 267.
Menten, K. M., Walmsley, C. M., Henkel, C., Wilson, T. L., Snyder, L. E., Hollis, J. M., and Lovas, F. J. 1986*b*, *Astr. Ap.*, **169**, 271.
Menten, K. M., Walmsley, C. M., Wilson, T. L., and Henkel, C. 1989, in *Molecular Clouds in the Milky Way and External Galaxies*, ed. R. L. Dickman, R. L. Snell, and J. S. Young (Berlin: Springer), p. 261.
Mezger, P. G., Chini, R., Kreysa, E., Wink, J. E., and Salter, C. J. 1988, *Astr. Ap.*, **191**, 44.
Morimoto, M., Ohishi, M., and Kanzawa, T. 1985, *Ap. J.* (*Letters*), **288**, L11.
Nakano, M., and Yoshida, S. 1986, *Pub. Astr. Soc. Japan*, **38**, 531.
Ohishi, M. 1984, Ph.D. thesis, University of Tokyo.
Ohishi, M., Kaifu, N., Suzuki, H., and Morimoto, M. 1986, *Ap. Space Sci.*, **118**, 405.
Padin, S., *et al.* 1989, *Ap. J.* (*Letters*), **337**, L45.
Plambeck, R. L., and Wright, M. C. H. 1988, *Ap. J.* (*Letters*), **330**, L61.
Rodríguez, L. F., Cantó, J., and Moran, J. M. 1982, *Ap. J.*, **255**, 103.
Schneps, M. H., Lane, A. P. Downes, D., Moran, J. M., Genzel, R., and Reid, M. J. 1981, *Ap. J.*, **249**, 124.
Szczepanski, J. C., Ho, P. T. P., Haschick, A. D., and Baan, W. A. 1989, in *The Center of the Galaxy*, ed. M. Morris (Dordrecht: Kluwer), p. 383.
Walmsley, C. M., Batrla, W., Matthews, H. E., and Menten, K. M. 1988, *Astr. Ap.*, **197**, 271.
Wilson, T. L., Johnston, K. J., Henkel, C., and Menten, K. M. 1989, *Astr. Ap.*, **214**, 321.
Woody, D. P., *et al.* 1989, *Ap. J.* (*Letters*), **337**, L41.

WILLEM A. BAAN: Arecibo Observatory, Arecibo, PR 00612

AUBREY D. HASCHICK: Haystack Observatory, Westford, MA 01886

KARL M. MENTEN: Harvard–Smithsonian Center for Astrophysics, 60 Garden Street, Cambridge, MA 02138